Supporting Information of :

Electrodeposited ZnO nanoparticles on vertically aligned carbon nanotubes (VACNTs) as promising charge extracting electrodes for halide perovskite devices

Raphaëlle Belchi[1,2], Baptiste Pibaleau[1], Mathieu Pinault[1], Bernard Ratier[2], Nathalie Herlin-Boime[1]*, Johann Bouclé[2]*

[1] *Université Paris-Saclay, CEA, CNRS, NIMBE, 91191 Gif-sur-Yvette, France*

[2] *Univ. Limoges, CNRS, XLIM, UMR 7252, F-87000 Limoges, France*

* Corresponding authors: johann.boucle@unilim.fr; nathalie.herlin@cea.fr

Materials & Methods: *Characterization Details*

Scanning Electron Microscopy (SEM) was performed on a SEM-FEG Zeiss Ultra 55 model to study the morphology, quality and thickness of the CNTs carpets. SEM was also performed to study the morphology of the electro-deposited ZnO and Perovskite crystals. The spatial distribution of ZnO/perovskite within the VACNTs can be monitored by mean of an EDX chemical analysing system (BRUCKER SDD detector) interfaced with the ESPRIT software.

Raman spectroscopy (SEM) was performed using a 532 nm green laser (XploRA PLUS - Horiba) to probe the structural properties of ZnO.

X-Ray Diffraction (XRD) was conducted in Bragg-Brentano geometry with a Bruker D8-ADVANCE (copper cathode) to obtain information regarding ZnO crystallinity.

Photoluminescence Spectroscopy (PL) was carried out in steady-state conditions. Spectra were measured in the 700-820 nm range using FLS980 spectrometer (Edinburg Instruments, UK). The excitation at 470 nm is provided by a monochromated 450W Xenon lamp and the detection operated by a cooled R928P Hamamatsu photomutiplier.

Current-Voltage (I-V) characteristics were recorded in ambient conditions (around 50% of relative humidity and in ambient air) on un-capsulated devices, using standard contact tips linked to a calibrated Keithley 2400 source-measure unit.

Results & Discussion

1. Perovskite Infiltration Study

1.1. Example of perovskite infiltration into low density (10^9CNTs/cm²) VACNTs

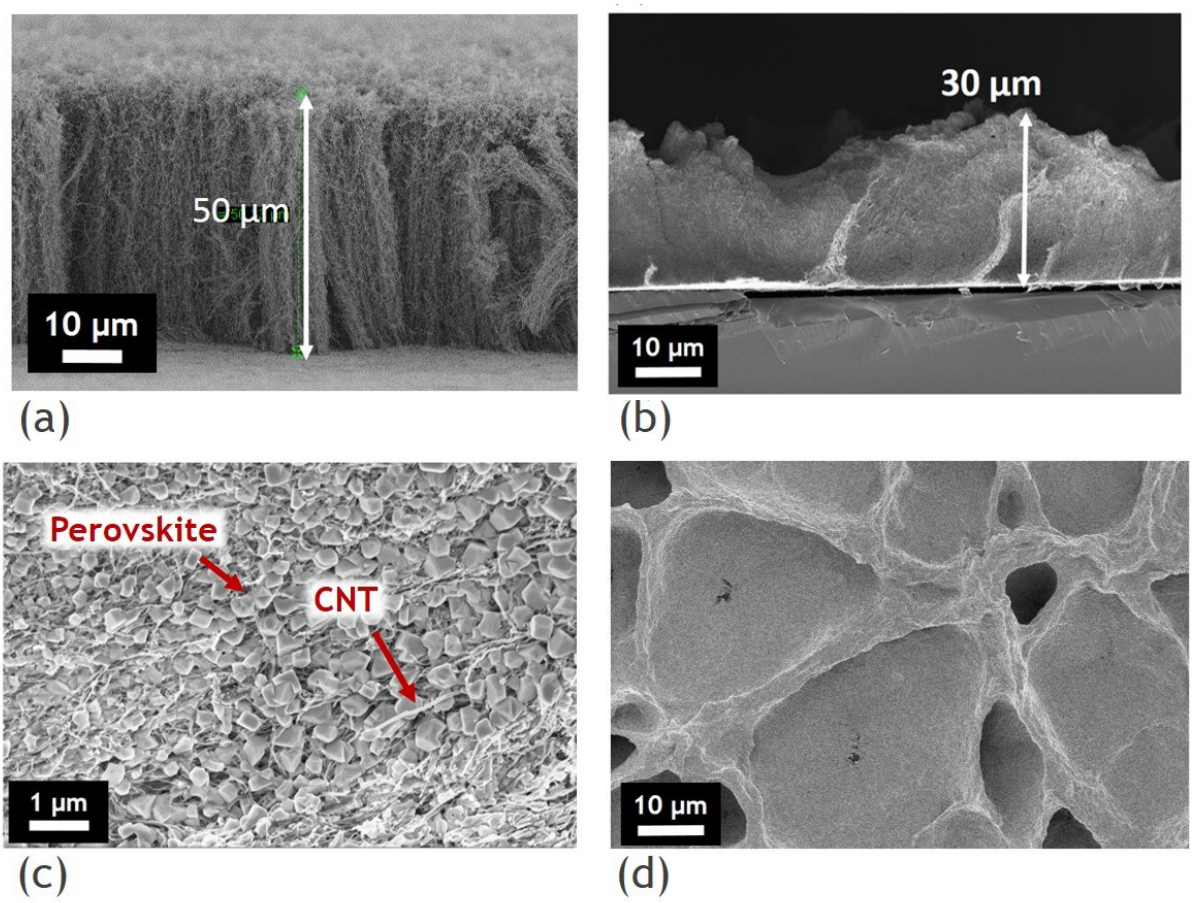

Figure S1 SEM images of (a) low density VACNTs carpet – cross-section (b) VACNTs after perovskite ($CH_3NH_3PbI_3$) two-step deposition – cross-section (c) zoom on the association between the perovskite crystals and CNTs (d) top-view of the sample : cavities are created by the solvent evaporation during perovskite deposition

Figure S1 present low density VACNTs networks obtained in Si substrates at 850°C. Our study revealed that the density of VACNTs is a key parameter to achieve high quality layers after perovskite deposition. Indeed, we emphasized that low density VACNTs network (10^9 CNTs/cm²) alignment is altered during the solvent evaporation occurring during the perovskite crystallization. A clear disruption of nanotubes alignment is observed in this case, as we can see on Figure S1 (b). Indeed, we can see on Figure S1 (d) typical cavities created by the solvent evaporation during perovskite deposition on low density VACNTs carpets. Nevertheless, Figure S1 (c) shows an intimate association between the carbon nanotubes and perovskite crystals that illustrates a good perovskite capability to infiltrate and crystallize despite the

low intertube space.

1.2. Influence of the perovskite deposition steps

Different classic perovskite deposition methods, widely reported in the literature, have been tested on low density (10^9 CNTs/cm²) dense VACNTs carpets. [1–3] Main results are summed up in Figure S2. Figure S2 (a) and (b) correspond to the sample after a two-step deposition (spin-coating followed by dip-coating) of classic methylammonium lead-iodide (MAPI) perovskite. Figure S2 (c) and (d) correspond to the same perovskite deposited in a single step (spin-coating). Finally, Figure S2 (e) and (f) correspond to a chloride methylammonium lead-iodide (MAPI-Cl) perovskite also deposited in one-step (spin-coating).[4] In all cases, grooves are created by the solvent evaporation during perovskite deposition. However, this phenomenon is more drastic for MAPI or MAPI-Cl deposited in one-step than for MAPI deposited in two-step. Moreover, the mixing between the perovskite and the CNTs seems to be more homogenous after a two-step deposition that lead to small geometrical crystals of perovskite (see Figure S2 (b)). Indeed we can see on Figure S2 (d) and (f) that the carbon nanotubes are completely entangled, losing the initial preferential orientation of VACNTs, whereas the perovskite is present as grains dispersed in random areas. Thus, it results from this observation that it seems preferable to use a two-step deposition process than a one-step process to infiltrate perovskite into VACNTs networks.

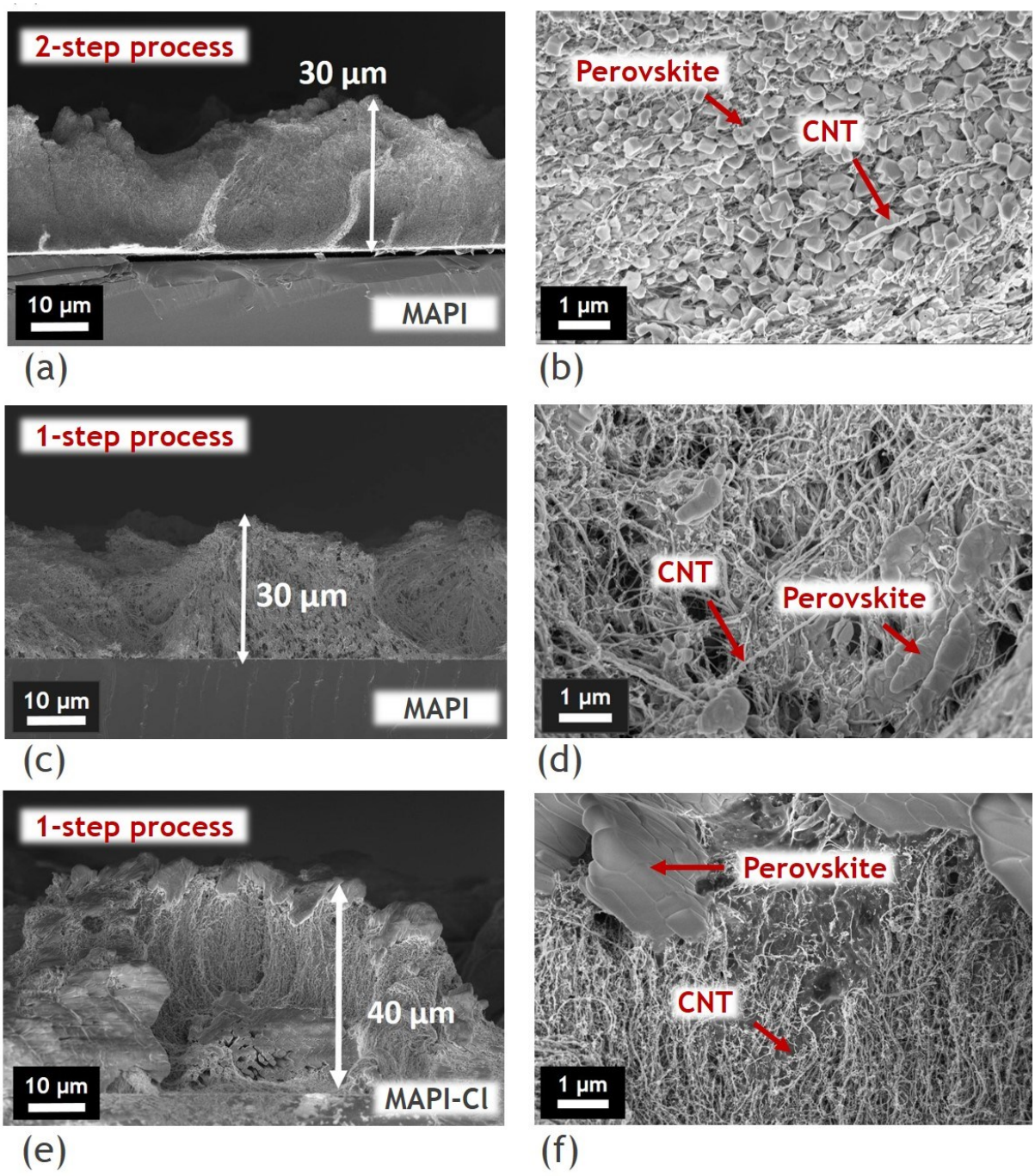

Figure S2 SEM images of 10^9CNTs/cm² density VACNTs – cross-section after perovskite deposition (a) and (b) $CH_3NH_3PbI_3$ (MAPI) two-step process (c) and (d) $CH_3NH_3PbI_3$ (MAPI) one-step process (e) and (f) $CH_3NH_3PbI_{3-x}Cl_x$ (MAPI-Cl) one-step process

2. Materials properties

As mentioned in the main article, a thermal annealing at 450°C is systematically performed during 5 minutes on the Al/VACNTs/ZnO sample to ensure an optimal crystallization of the ZnO and avoid residual hydroxyl groups that could be present after the electrodeposition and are known to cause perovskite degradation. X-Ray Diffraction before and after thermal annealing is presented in Figure S3. The measurements revealed a decrease of Full-Width Half-Maximum (FWHM) of the peaks, evidencing an improvement of the ZnO nanoparticles crystallinity with the annealing.

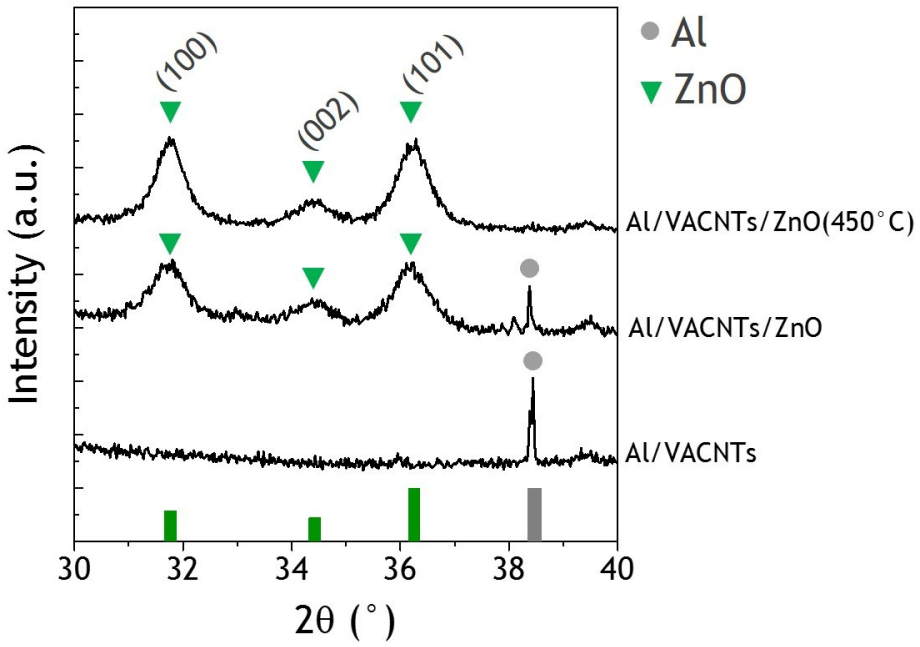

Figure S3 XRD diagrams of Al/VACNTs, Al/VACNTs/ZnO and Al/VACNTs/ZnO after 450°C thermal annealing (copper cathode, Bragg-brentano configuration)

ZnO nanoparticles signature is also detected after thermal annealing by Raman spectroscopy at 405 cm^{-1}, 434 cm^{-1} and 575 cm^{-1} that correspond respectively to the A_{1LO}, E_2 and E_{1LO} modes, as shown in Figure S4.

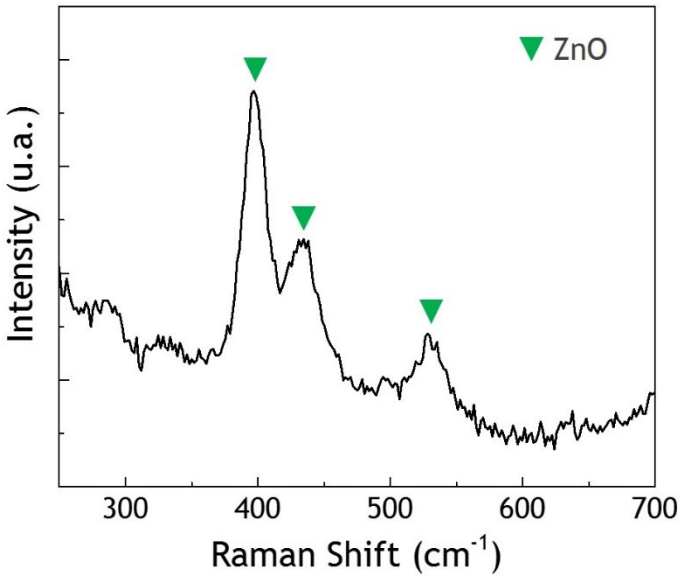

Figure S4 Raman spectroscopy (532 nm LASER) of Al/VACNTs after ZnO electrodeposition and thermal annealing (450 °C) – contributions at 400 cm^{-1}, 434 cm^{-1} and 532 cm^{-1} corresponding to ZnO signature

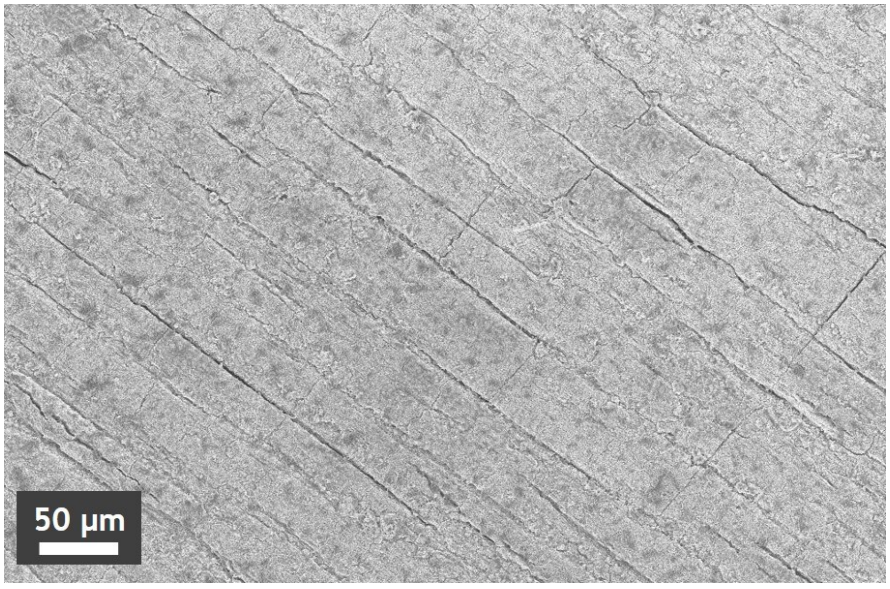

Figure S5 SEM image (top view) of the Al/VACNTs sample after ZnO electrodeposition and thermal annealing (450°C). The sample is still compact and homogeneous and VACNTs are completely covered by ZnO nanoparticles

3. Fabrication of a test device

This section gives more details about the comparison between Al/VACNTs and Al/VACNTs/ZnO systems, highlighting the relevance of using ZnO nanoparticles along the CNTs. Figure S6 shows the results of perovskite infiltration and crystallization into high density (10^{11} CNTs/cm²) VACNTs carpets, with and without ZnO nanoparticles. In both cases, perovskite solution managed to infiltrate the

VACNTs network leading to a homogeneous crystallization from the bottom to the top of the carpets. Nevertheless, the sample containing ZnO nanoparticles provides a better conservation of the CNTs alignment and is much more compact.

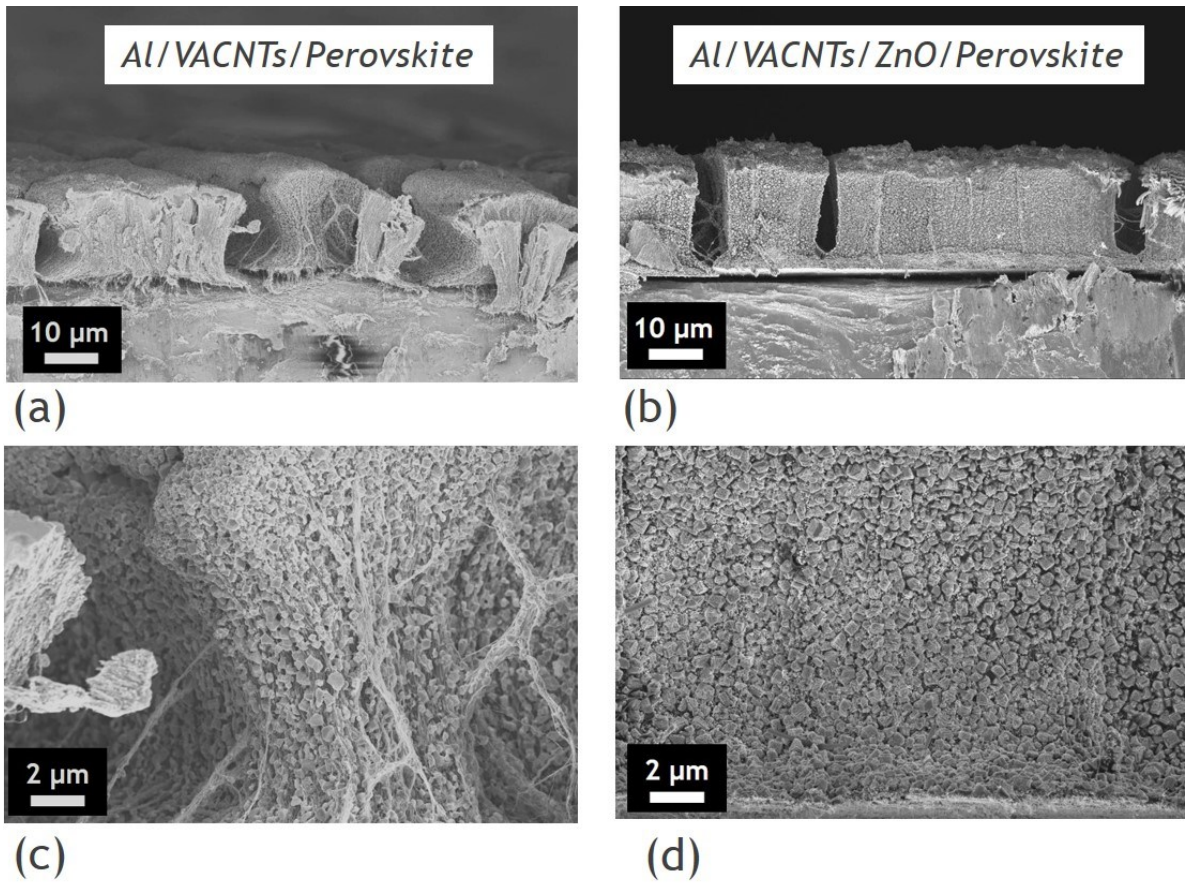

Figure S6 (a) and (c) Al/VACNTs after perovskite deposition at different magnifications (b) and (d) Al/VACNTs/ZnO after perovskite deposition at different magnifications – The sample containing ZnO provides a better conservation of CNTs alignment and is more compact

Details of Spiro-OMeTAD layer deposition

A hole transport material has been deposited onto the perovskite (see Figure S7), by drop-casting of 10 µL of a Spiro-OMeTAD solution.

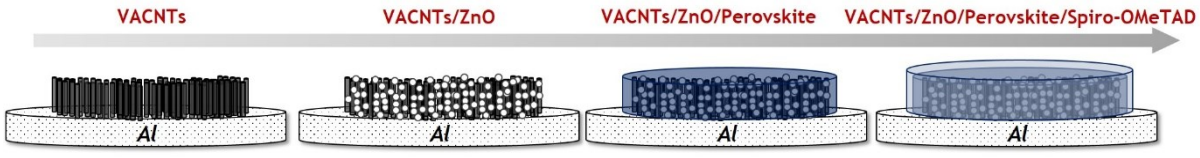

Figure S7 Scheme of the sample after the different materials depositions

The Figure S8 presents the morphology after Spiro-OMeTAD deposition on Al/VACNTs/Perovskite and Al/VACNTs/ZnO/Perovskite samples. As we can see on Figures (a), (b) and (c), the sample based

on VACNTs presents large grooves and heterogeneity, whereas the VACNTs/ZnO based sample is more compact with an homogeneous covering of the hole transport material.

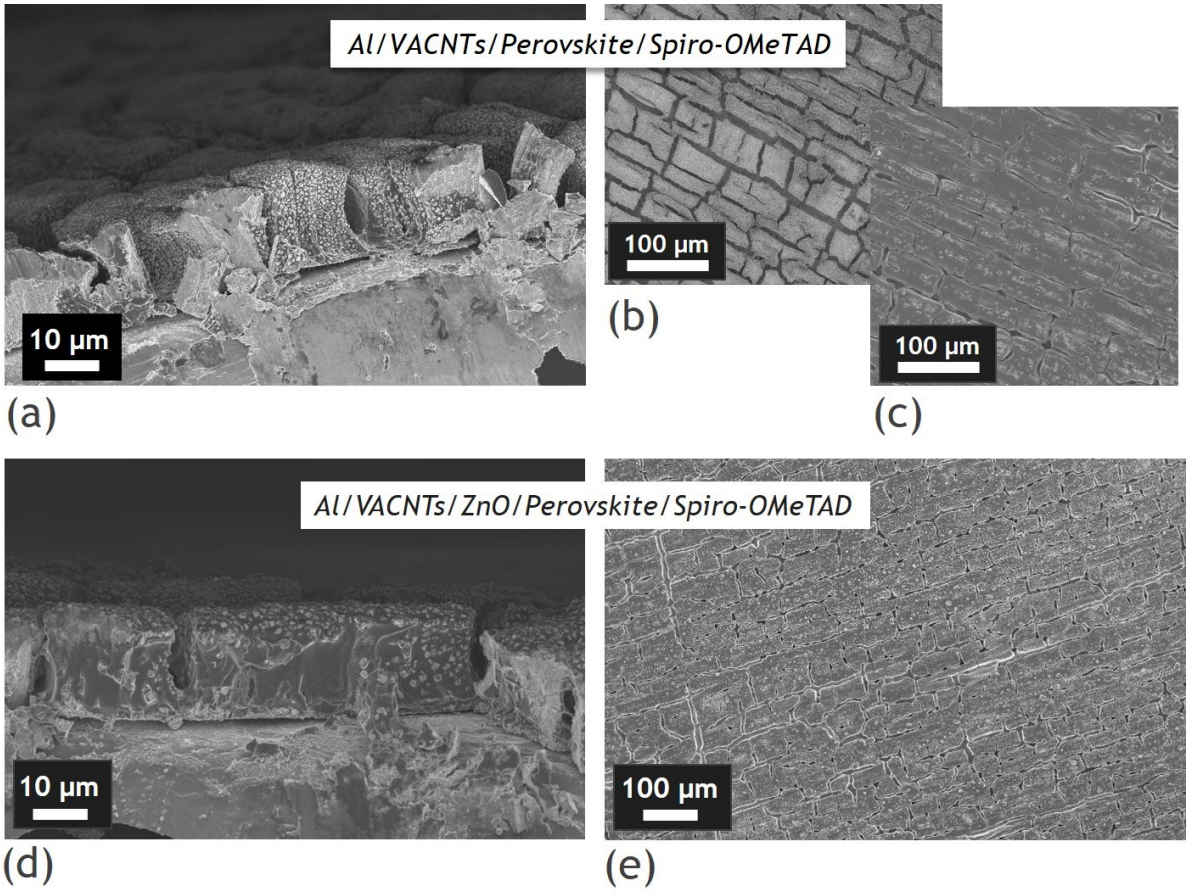

Figure S8 SEM (a) cross-section (b) and (c) top-view of the Al/VACNTs/ Perovskite sample after Spiro-OMeTAD deposition (d) cross-section (e) top-view of the Al/VACNTs/ZnO/Perovskite sample after Spiro-OMeTAD deposition

The heterogeneities observed for the Al/VACNTs based electrode can explain the difference of behaviour between the two samples during I-V measurements, as shown in Figure S9. Indeed, we can see on Figure S9 (a) that the ZnO-free sample behaves as an ohmic conductor with a resistance around 8 Ω, whereas the ZnO-containing sample has a diode-like behavior. Moreover, the Figure S9 (b) evidences a higher leakage current in case of the ZnO-free electrode.

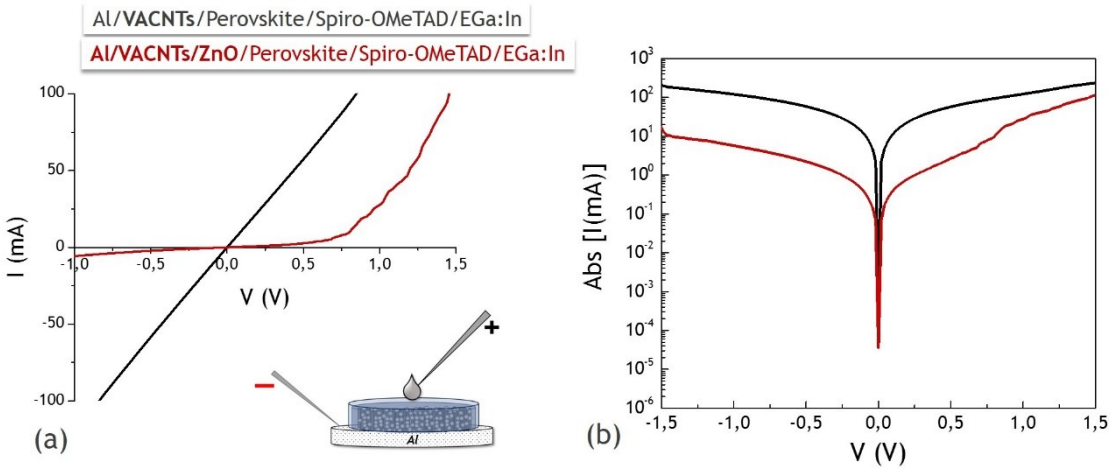

Figure S9 (a) I-V dark measurment of Al/VACNTs/ Perovskite/Spiro-OMeTAD/EGa:In and Al/VACNTs/ZnO/Perovskite/Spiro-OMeTAD/EGa:In – 0,0079 cm² active areas (b) semi-logaritmic representations

However, we must point out here that the results obtained for the ZnO-free device, do not come from a material issue but mainly from the strong inhomogeneity of the layer after perovskite infiltration (this is an engineering problem) that could still be improved by avoiding short-circuits with optimized layers depositions.

1. References

1 J. Lee and N. Park, *MRS Bull.*, 2015, **40**, 654–659.

2 I. Mesquita, L. Andrade and A. Mendes, *Renew. Sustain. Energy Rev.*, 2018, **82**, 2471–2489.

3 P. Tonui, S. O. Oseni, G. Sharma, Q. Yan and G. Tessema Mola, *Renew. Sustain. Energy Rev.*, 2018, **91**, 1025–1044.

4 R. Belchi, A. Habert, E. Foy, A. Gheno, S. Vedraine, R. Antony, B. Ratier, J. Bouclé and N. Herlin-boime, *ACS Omega*, 2019, **4**, 11906–11913.